In MICCAI 2003 proceedings
LNCS 2878: 108-115

Medially Based Meshing with Finite Element Analysis of Prostate Deformation

Jessica R. Crouch[1], Stephen M. Pizer[1], Edward L. Chaney[1], and Marco Zaider[2]

[1] Medical Image Display & Analysis Group,
University of North Carolina at Chapel Hill
[2] Memorial Sloan-Kettering Cancer Center

Abstract. The finite element method (FEM) is well suited for use in the non-rigid registration of magnetic resonance spectroscopy images (MRSI) with intraoperative ultrasound images of the prostate because FEM provides a principled method for modeling the physical deformation caused when the MRSI intra-rectal imaging probe compresses the prostate. However, FEM requires significant labor and computational time to construct a finite element model and solve the resulting large system of equations. In particular, any finite element based registration method must address the questions of how to generate a mesh from an image and how to solve the system of finite element equations efficiently. This paper focuses on how m-rep image segmentations can be used to generate high quality multi-scale hexahedral meshes for use with FEM. Results from the application of this method to the registration of CT images of a prostate phantom with implanted brachytherapy seeds are presented.

1 Introduction

This paper considers finite element techniques for non-rigidly registering three-dimensional prostate images acquired for the purpose of brachytherapy planning and guidance. Brachytherapy involves implanting radioactive seeds in the prostate to treat prostate cancer. A magnetic resonance spectroscopy image (MRSI) can be used to design a seed placement pattern that targets suspected tumor deposits, but the process is complicated by the fact that the prostate appears compressed in the MRSI due to pressure from the intra-rectal imaging probe. Intra-operatively, the prostate is not deformed and seed placement is guided using ultrasound. Therefore, a non-rigid image registration is required to match points within the prostate shown in the MRSI planning image with the corresponding points in the intra-operative ultrasound image.

Other researchers have approached prostate imaging problems using methods that incorporate finite element analysis, in particular [4] and [8]. The work presented in [4] is most similar to the algorithm presented here, but differed from ours in that it relied on manual segmentation and tetrahedral meshing, and a membrane model of the boundary rather than a solid object model was used in the computation of boundary conditions. The work presented in [8] employed a combined statistical and biomechanical approach.

The registration process used in this work consists of the following steps.

1. Fit an m-rep medial model to the prostate in both the undeformed and deformed images.
2. Build a multiscale finite element mesh from one of the models.
3. Derive boundary conditions that produce the observed shape change and minimize the energy of the deformation.
4. Assume the prostate is a linearly elastic body and compute its deformation using finite element analysis.
5. Apply the computed deformation to the undeformed image to register it with the deformed image.

Section 2 details how m-rep object models are used to automatically generate a mesh from an image. The derivation of boundary conditions is explained in section 3 and the solution algorithm is reviewed section 4. Registration results for CT images of a prostate phantom are presented in section 5. Some aspects of the registration algorithm are summarized in this paper due to space considerations. Further algorithmic details can be found in [5] for sections 2.3, 3, and 4.

2 Meshing Algorithm

2.1 M-Rep Geometry Models

The novel meshing algorithm presented here relies on m-rep object models to provide both global and local object shape information. M-reps are medially based solid models particularly well suited for modeling anatomic objects and segmenting medical images [9]. For this application, m-reps' object based coordinate system facilitates both the construction of the finite element mesh and the efficient solution of the finite element system of equations.

The prostate's shape can be well represented with a single figure m-rep, shown in Fig. 1(b). A figure is composed of a lattice of medial atoms, the smallest building blocks of an m-rep. Each atom stores a sample of object geometry, including the coordinates of a point on the medial surface, the object radius, the coordinates of at least two boundary points, and a frame that provides object orientation information.

The lattice arrangement of medial atoms helps define an object based coordinate system for m-reps. Any point in an object can be referenced by its m-rep defined (u, v, t, τ) coordinates. The u and v directions coincide with the rows and columns of medial atoms in the lattice. τ ranges between 0 at the medial surface and ± 1 at the object surface, while t measures the angle between a vector and the medial surface. This object based coordinate system provides spatial and orientational correspondence between deformed versions of the same object. This is advantageous in the meshing context because it means that a mesh defined using an m-rep's object based coordinates is automatically individualized to fit any deformed version of the m-rep model. Another benefit of the object based coordinate system is the ability to express distances as a fraction of object width. This is convenient for mesh generation as it provides a natural way to size elements according to the proportions of an object.

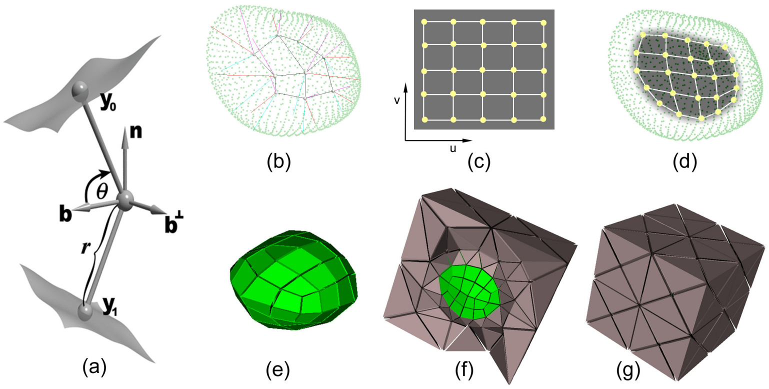

Fig. 1. (a) A diagram of a single medial atom (b) An m-rep prostate model constructed from 3x3 lattice of medial atoms. (c) The (u,v) parameter plane of the medial surface with a 5x5 grid of sample points indicated. (d) Object with sample point interpolated and drawn on the medial surface. (e) Base level prostate mesh (f) Sliced view of the meshed volume of interest (g) Exterior view of the meshed volume of interest

2.2 Hexahedral Meshing Algorithm

Research has shown that for linear elastic problems and non-linear elasto-plastic problems the error in a finite element solution is smaller for a mesh of linear hexahedral elements than for a mesh of similarly sized linear tetrahedral elements [3]. Current automatic meshing algorithms are more successful at constructing quality tetrahedral meshes than quality hexahedral meshes, and the development of general purpose automatic hexahedral meshing algorithms is a problem that motivates current research efforts in the meshing community [11].

A quality hexahedral finite element mesh must have several characteristics.

- Compatibility – Interior faces must be shared by adjoining elements. This assures monotonic convergence of the finite element equations [2].
- Good element shape – If an element is inverted or the mesh folds, a valid finite element solution does not exist. Severely skewed elements negatively affect the convergence characteristics of the finite element system of equations.
- Boundary fitted – The accuracy of the finite element solution is limited by how closely the mesh approximates the object's geometry.

Promising hexahedral meshing algorithms have employed information about global object shape in the mesh design process. Price and Armstrong's work decomposed an object into a set of geometric primitives using the medial axis [10]. A more recent introduction was whisker weaving, an algorithm that uses the spatial twist continuum to design a three dimensional hexahedral mesh that conforms to a specified quadrilateral surface mesh for an object [6] [12].

The m-rep based meshing algorithm uses a standardized meshing pattern for each figure and assigns object coordinates to each node. The mapping from object based coordinates to world space coordinates determines the nodes' world space positions.

Fig. 2. Three groups of nodes are constructed from three corresponding medial surface samples. a_0 and b_0 are samples on the center portion of a medial surface and give rise to nodes a_0 - a_4 and b_0 - b_4. c_0 is a sample on the outer rim of the medial surface, from which nodes c_0 - c_5 are constructed.

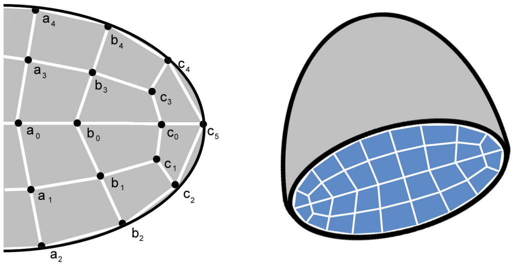

The first step in meshing an m-rep figure is the construction of a sampling grid on the (u, v) parameter plane of the medial surface. The vertices of the sampling grid are placed at regular intervals in (u, v) coordinates, and their world space coordinates are calculated by interpolating a position on the medial surface. The spacing is determined by the ratio of the average object thickness to the average distance between medial atoms. Using this spacing, the average hexahedral element will have roughly equal dimensions.

From the sampling grid on the medial surface, the coordinates of the other layers of nodes can be derived. For every (u, v) sample point except those around the outer rim of the medial lattice, five nodes are created at $\tau = -1, -.5, 0, .5, 1$. For sample points around the lattice edge, a set of six nodes is created, with the sixth node sitting out on the object crest. The node and element patterns are illustrated in Fig. 2.

Although the sample spacing is regular in medial coordinates, when the mesh is mapped into world space (x, y, z) coordinates the elements in narrower regions of the object tend to be smaller than the elements in wider areas. Typically this is a desirable property, since a mesh usually needs to have smaller elements in narrower parts of an object in order to sufficiently model the detail. Because the mesh construction is guided entirely by information contained in the m-rep model, the meshing process requires no user interaction.

2.3 Mesh Quality Optimization

The shape quality of the majority of elements generated by the m-rep meshing algorithm is good, but elements created near the corners of the parameterized medial surface or in areas of high curvature can be more skewed than elements in the central portion of a model. To correct this, the positions of some of nodes are adjusted in an optimization of an element quality measure. In this process, nodes on the surface of an object have two degrees of freedom and are constrained to remain on the surface. Nodes in the interior of an object have three degrees of freedom. The optimization ensures that the mapping between the elements' parameter space and world space is well defined and does not fold.

2.4 Mesh Subdivision

Mesh subdivision can be applied to increase solution accuracy. Subdividing produces a mesh with smaller elements that provide a finer representation of the

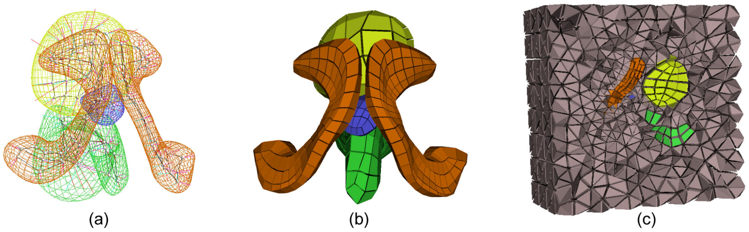

Fig. 3. (a) M-rep model of male pelvis, including pubic bones, rectum, bladder, and prostate (b) Mesh of male pelvis objects (c) Sliced view of object meshes with connecting pyramid and tetrahedral elements filled in

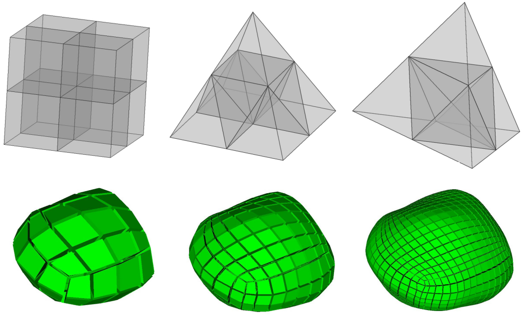

Fig. 4. Top Row: Element subdivision patterns for hexahedra, pyramid, and tetrahedra elements.

Bottom Row: Three subdivision levels of a prostate mesh.

solution. The subdivision algorithm involves creating new nodes at the centers of each existing edge, quadrilateral face, and hexahedral volume in the mesh. Fig. 4 shows the subdivision pattern for the three element types.

The hexahedral elements that represent the m-rep modeled objects have nodes with both world space (x, y, z) coordinates and medial (u, v, t, τ) coordinates. By subdividing these elements using their medial node coordinates, an improved, smoother approximation to the object geometry is achieved with subdivision. In contrast, subdivision using world space coordinates would provide improved resolution for representing the solution but would not reduce the geometric error or blockiness of the mesh. The medial coordinate based subdivision process allows for increased precision in both the geometry and the solution.

If adjacent faces of an element lie on the object surface, then the subdivision process described would lead to increasingly distorted and flattened elements since any surface patch is flat at a sufficiently small scale. The meshing pattern presented here has no elements with more than one face lying on the object boundary, thus allowing good element shape to be maintained through an arbitrary number of mesh subdivisions.

2.5 Meshing Space External to M-reps

By meshing the space outside and between m-rep modeled objects, a deformation can be interpolated into the surrounding space. External space meshing begins by building a layer of non-intersecting pyramids on top of the exposed quadrilateral faces of a hexahedral figure mesh. Tetrahedra are then built on top of the exposed triangular faces of the pyramids and used to mesh the remainder of the volume of interest. The construction of the tetrahedral mesh is performed using the tetrahedral meshing capability found in CUBIT [1]. Subdivision of these pyramid and tetrahedral elements is performed using the nodes' world space (x,y,z) coordinates and the pattern illustrated in Fig. 4.

3 Boundary Conditions

In order to compute a deformation with finite elements, boundary conditions must be specified either in terms of forces applied to nodes or node displacements. With an image registration problem, neither forces nor point displacements are available directly from the images. What is visible is shifting and/or change in boundary shape. M-reps provide a way to derive an initial approximation to point displacements from observed boundary changes in an image.

In the prostate case, the m-rep model that was fit to the original image and used to guide mesh construction is transferred onto the image of the deformed prostate and adapted to fit it. The original and deformed m-rep models have the same object based coordinate space so that a one to one mapping is defined between points in the original and deformed prostate. This correspondence defines an initial set of boundary node displacements.

The boundary conditions are optimized by minimizing the physical energy of the computed deformation. This approach is based on the assumption that given the set of all possible boundary conditions that produce the observed shape change, the one requiring the least energy is most likely. In the optimization process the correspondence between points on the surface of the original m-rep and points on the surface of the deformed m-rep is refined by allowing the points on the deformed m-rep to slide along its surface.

4 Solution Algorithm

To compute a deformation, an NxN system of linear equation must be solved, where N is the number of nodes in the mesh. An initial approximation to the solution can be derived from the m-rep models by making use of the correspondence that exists between deformed versions of an m-rep. A conjugate gradient algorithm is used to improve the approximate solution to within a set tolerance.

The system of equations that results from a subdivided mesh is much larger than the original system of equations, as seen in Table 1. The larger system of equations can be efficiently solved by borrowing the idea from multigrid theory of solving the problem using meshes at different scales. The approach taken here is to solve the system of equations on the coarsest mesh, and then interpolate that solution to the next mesh level and improve the solution iteratively with a conjugate gradient algorithm. The number of iterations required to converge to a solution on a high resolution mesh is reduced due to the good solution approximation computed for a coarser mesh level. At subdivision level 3, the solution prediction scheme reduces the number of solution iterations by half.

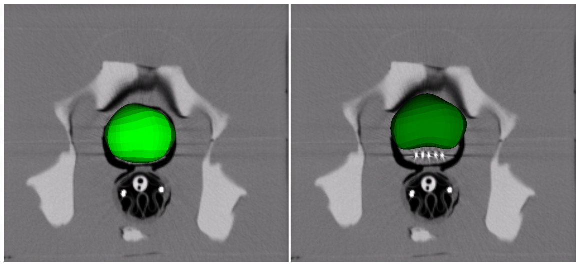

Fig. 5. Left: Original mesh of the prostate superimposed on a slice of the uninflated CT image.

Right: Deformed mesh of the prostate superimposed on the same slice.

5 Registration Experiment

The initial validation study of the registration methodology was performed using CT images of a prostate phantom. The phantom prostate was implanted with seeds, and images were acquired with an inflated and deflated MRSI probe in place. The accuracy of the computed deformation can be evaluated by comparing computed seed displacements with observed seed displacements. For this test, the prostate was the only pelvic structure explicitly modeled with an m-rep, and the surrounding area was represented as an elastic, homogeneous region. The linear elastic model has two elastic constants that characterize a material's stiffness: E, Young's modulus, and ν, Poisson's ratio. In this experiment the prostate was assigned $E = 60kPa$ and $\nu = .495$ based on the prostate tissue test results published in [7]. The area exterior to the prostate was assigned $E = 10kPa$ and $\nu = .495$.

The locations of 75 seeds in the phantom prostate were identified manually in both the uninflated and inflated CT images with .3 cm slice thickness and .07 cm within slice resolution. The computed deformation was applied to the seed locations in the uninflated image to predict the seed locations in the inflated image. The error estimates in Table 1 were derived by comparing predicted seed locations with observed seed locations in the inflated probe image. The accuracy of manual seed labelling was limited by the image resolution, and to the extent that errors in seed coordinates contributed to the error estimates, the estimates indicate a limitation of the validation procedure rather than a limitation of the registration methodology.

Table 1. Error estimates for predicted seed locations in cm. x and y components lie in a high resolution image plane, and the z component lies across the image planes.

mesh subdivision level	node count	total error	total std. dev.	x error	x std. dev.	y error	y std. dev.	z error	z std. dev.
1	254	.2705	.0869	.1308	.0785	.1026	.0776	.1730	.1057
2	1,836	.2054	.0799	.0852	.0605	.0679	.0547	.1485	.0900
3	14,068	.2000	.0807	.0766	.0580	.0761	.0598	.1393	.0928

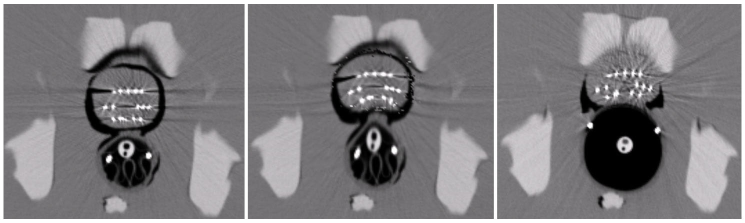

Fig. 6. Left: original slice of uninflated probe image. Center: slice after computed deformation was applied. Right: comparison slice from image with inflated probe

6 Acknowledgements

This work was supported by NIH grant CA P01 47982 and by a Lucent GRPW fellowship. The authors thank Gregg Tracton for image processing assistance and Gilad Cohen for the phantom design.

References

1. CUBIT information available at http://endo.sandia.gov/cubit/.
2. K Bathe. *Finite Element Procedures.* Prentice-Hall, New Jersey, 1996.
3. S E Benzley, E Perry, K Merkley, B Clark, and G Sjaardama. A comparison of all hexagonal and all tetrahedral finite element meshes for elastic and elasto-plastic analysis. *Proc., 4th Intl. Meshing Roundtable*, pages 179–191, October 1995.
4. A Bharatha, M Hirose, N Hata, S Warfield, M Ferrant, K Zou, E Suarez-Santana, J Ruiz-Alzola, A D'Amico, R Cormack, R Kikinis, F Jolesz, and C Tempany. Evaluation of three-dimensional finite element-based deformable registration of pre-and intraoperative prostate imaging. *Medical Physics*, 28:2551–2560, Dec 2001.
5. J Crouch, S Pizer, E Chaney, and M Zaider. Medial techniques to automate finite element analysis of prostate deformation. *submitted to: IEEE Transactions on Medical Imaging*, Feb 2003. http://www.cs.und.edu/ jrc/TMI_JRC.pdf.
6. N T Folwell and S A Mitchell. Reliable whiskerweaving via curve contraction. *Proceedings, 7th International Meshing Roundtable*, pages 365–378, October 1998.
7. T A Krouskop, T Wheeler, F Kallel, B Garra, and T Hall. Elastic moduli of breast and prostate tissues under compression. *Ultrasonic Imaging*, 20:260–274, 1998.
8. A Mohamed, C Davatzikos, and R Taylor. A combined statistical and biomechanical model for estimation of intra-operative prostate deformation. *MICCAI*, pages 452–460, 2002.
9. S M Pizer, J Z Chen, P T Fletcher, Y Fridman, D S Fritsch, A G Gash, J M Glotzer, M R Jiroutek, S Joshi, C Lu, K E Muller, A Thall, G Tracton, P Yushkevich, and E L Chaney. Deformable m-reps for 3D medical image segmentation. *International Journal of Computer Vision*, submitted Sept. 2002. http://midag.cs.unc.edu/pubs/papers/IJCV01-Pizer-mreps.pdf.
10. M A Price and C G Armstrong. Hexahedral mesh generation by medial surface subdivision: Part II. solids with flat and concave edges. *International Journal for Numerical Methods in Engineering*, 40:111–136, 1997.
11. R Schneiders. Quadrilateral and hexahedral element meshes. In Thompson, Soni, and Weatherill, editors, *Handbook of Grid Generation.* CRC Press, Florida, 1998.
12. T J Tautges and S Mitchell. Progress report on the whisker weaving all-hexahedral meshing algorithm. *Proc. 5th International Conference on Numerical Grid Generation in Computational Fluid Simulations*, pages 659–670, 1996.